Reprinted from **Applied Optics**, Vol. 22, page 3001, October 1, 1983


# Light scattering by randomly oriented cubes and parallelepipeds

K. N. Liou, Q. Cai, J. B. Pollack, and J. N. Cuzzi

In this paper, we have modified the geometric ray tracing theory for the scattering of light by hexagonal cylinders to cubes and parallelepipeds. Effects of the real and imaginary parts of the refractive index and aspect ratio of the particle on the scattering phase function and the degree of linear polarization are investigated. Causes of the physical features in the scattering polarization patterns are identified in terms of the scattering contribution due to geometric reflections and refractions. The single-scattering phase function and polarization data presented in this paper should be of some use for the interpretation of observed scattering and polarization data from planetary atmospheres and for the physical understanding of the transfer of radiation in an atmosphere containing nonspherical particles.

## I. Introduction

Knowledge of the single-scattering parameters involving atmospheric particulates is needed for the understanding of the transfer of solar and IR radiation in planetary atmosphers and the development of remote sensing techniques for their identification. In recent years, the influence of nonspherical particles such as ice crystals and aerosols on the radiation budget of the atmosphere and hence climate has been a subject of considerable research interest and scientific importance.

Since exact Mie-type solutions for the scattering of electromagnetic waves by nonspherical particles have been analytically derived and numerically tested only for symmetrical particles with smooth surfaces such as spheroids,[1,2] it is necessary to develop alternate approaches, e.g., based on optical principles, to evaluate approximately the single-scattering characteristics of irregularly shaped aerosols, hexagonal ice crystals, and other types of nonspherical particle which are present in planetary atmospheres. Pollack and Cuzzi,[3] for example, developed a semiempirical theory for scattering by randomly oriented micron-sized nonspherical particles based on simple physical principles and comparisons with laboratory scattering data for cubes and other types of irregular particle. Recently, Cai and Liou[4] (CL) developed a theory for the scattering of polarized light by hexagonal ice crystals utilizing the geometric ray tracing technique. In this paper, we wish to extend this theory to rectangular parallelepipeds and cubes. While such a theory is known to be extremely accurate for sufficiently large ratios of particle size to the wavelength (say $\gtrsim 1000$), the calculations of Pollack and Cuzzi suggest that it may be a useful approximation for much smaller size ratios (say $\gtrsim$ several). We put this possibility to test by comparing our calculations to laboratory data for small sized randomly oriented cubes.

K. N. Liou and Q. Cai are with University of Utah, Meteorology Department, Salt Lake City, Utah 84112; the other authors are with NASA Ames Research Center, Space Science Division, Moffett Field, California 94035.

Received 21 March 1983.

## II. Geometric Ray Racing Analysis

We apply the geometric ray tracing analyses presented by CL for hexagonal cylinders to rectangular parallelepipeds. Except for the plane equations and associated direction cosines, the basic equations and procedures governing the ray tracing are exactly the same as in the hexagon case. Let $a$, $b$, and $h$ denote length, width, and height of a rectangular parallelepiped, respectively. The plane equations which describe the six surfaces ($n$ = 0,1,2,3,4,5) denoted in Fig. 1 with respect to the $OXYZ$ coordinate system may be written, respectively, as

$$\left.\begin{aligned} x &= b/2 \\ y &= a/2 \\ x &= -b/2 \\ y &= -a/2 \\ z &= h/2 \\ z &= -h/2 \end{aligned}\right\} \quad (1)$$

The associated direction cosines of the normals for the surfaces are given by

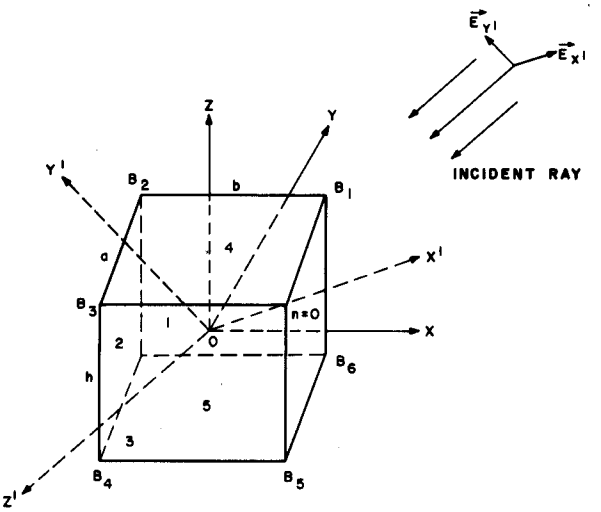


Fig. 1. Geometry of the orientation of a parallelepiped with respect to the incident electric vector of a geometric ray. The incident electric vector is described by the $OX'Y'Z'$ coordinate, while the orientation of the rectangle is fixed in the $OXYZ$ coordinate.

$$\left.\begin{aligned}\cos\alpha_n &= \cos n\pi/2\\ \cos\beta_n &= \sin n\pi/2\\ \cos\gamma_n &= 0\end{aligned}\right\} n = 0,1,2,3,$$

$$\left.\begin{aligned}\cos\alpha_n &= 0\\ \cos\beta_n &= 0\\ \cos\gamma_n &= \cos[(n-4)\pi]\end{aligned}\right\} n = 4,5, \tag{2}$$

where $\alpha$, $\beta$, and $\gamma$ are the angles between the outward directed normals and the $X$, $Y$, and $Z$ coordinates, respectively, and $n = 0$ denotes the surface perpendicular to the $OX$ axis. The other three-side surfaces are successively represented by $n = 1,2,3$, while $n = 4$ and 5 denotes the top and bottom surfaces.

Moreover, the general equation describing the Fraunhofer diffraction for the far field may be written[5]

$$u_p = \frac{-ju_0}{\lambda r}\int_{B'}\int \exp(-jkr)dx'dy', \tag{3}$$

where $u_0$ represents the disturbance in the original wave at point $O$ on the plane wave front with wavelength $\lambda$, $r$ is the distance between point $P$ in the far field and point $O'$ ($X'Y'$ coordinate) on the aperture with an area $B'$, $k = 2\pi/\lambda$, and $j = \sqrt{-1}$. The six apexes $B_i'$ ($i$ = 1–6) that define the aperture are the projections of the six vertices $B_i$ ($i$ = 1–6) of the rectangular parallelepiped on the plane perpendicular to an oblique incident light ray. These six vertices are given by $B_1(b/2,a/2,h/2)$, $B_2(-b/2,a/2,h/2)$, $B_3(-b/2,-a/2,h/2)$, $B_4(-b/2,-a/2,-h/2)$, $B_5(b/2,-a/2,-h/2)$, and $B_6(b/2,a/2,-h/2)$. Through a coordinate transformation, values of $B_i'$ may be obtained, and Eq. (3) may be integrated to give

$$u_p = \frac{-ju_0}{k^2\lambda r}\sum_{i=1}^{6}\left(\frac{g_i}{P_iC_i} - \frac{h_i}{P_iD_i}\right). \tag{4}$$

Equations for $g_i$, $h_i$, $P_i$, $C_i$, and $D_i$ are defined in CL.

According to the coordinate systems described by CL, we may express the scattered electric field for a rectangular parallelepiped in the form[6]

$$\begin{bmatrix}E_l\\ E_r\end{bmatrix}_{Z'OP} = \begin{bmatrix}A_2 & A_3\\ A_4 & A_1\end{bmatrix}\begin{bmatrix}E_{x0}'\\ E_{y0}'\end{bmatrix}_{Z'OX'}, \tag{5}$$

where $E_l$ and $E_r$ represent the parallel and perpendicular components of the scattered electric field, respectively, with respect to the scattering plane, and $E_{x0}'$ and $E_{y0}'$ are those of the incident electric field with respect to the incident plane. The amplitude functions $A_1$, $A_2$, $A_3$, and $A_4$ defined in Eq. (5) may be written as the sum of the diffraction $f$ and geometric reflection and refraction $s$ in the form

$$\mathbf{A} = \mathbf{A}^f + \mathbf{A}^s = \begin{bmatrix}A_2^f & A_3^f\\ A_4^f & A_1^f\end{bmatrix} + \begin{bmatrix}A_2^s & A_3^s\\ A_4^s & A_1^s\end{bmatrix}, \tag{6}$$

where the expression for $A^f$ and $A^s$ may be found in the paper by CL.

The Stokes parameters of the scattered light are given by

$$\begin{bmatrix}I\\ Q\\ U\\ V\end{bmatrix} = \mathbf{F}(\theta,\phi)\begin{bmatrix}I_0\\ Q_0\\ U_0\\ V_0\end{bmatrix}; \tag{7}$$

$\mathbf{F}(\theta,\phi)$ denotes the general transformation matrix given by van de Hulst.[6] The scattering phase function $P_{11}$ is defined by

$$P_{11} = \frac{4\pi}{\sigma_s}F_{11}, \tag{8}$$

where

$$F_{11} = \frac{1}{2}\sum_{k=1}^{4}|A_k|^2,$$

and the scattering cross section

$$\sigma_s = \int_0^{2\pi}\int_0^{\pi}(E_lE_l^* + E_rE_r^*)\sin\theta d\theta d\phi. \tag{9}$$

In this case the scattering phase function is said to be normalized so that

$$\int_{4\pi}P_{11}(\Omega)d\Omega/4\pi = 1. \tag{10}$$

The scattering phase function for an arbitrarily oriented nonspherical particle depends not only on the scattering $\theta$ and azimuthal $\phi$ angles with respect to the incident light rays but also on its orientation angles.[1,4] As shown by CL, two integration procedures are required to obtain the scattering phase function for randomly oriented parallelepipeds. The first angular integration is with respect to the angle denoting the orientation of the parallelepiped in reference to its long axis $\psi_1$ as follows:

$$P_{11}(\theta,\phi;\eta,\psi_2) = \frac{1}{2\pi}\int_0^{2\pi}P_{11}(\theta,\phi;\eta,\psi_2,\psi_1)d\psi_1, \tag{11}$$

where $\eta$ and $\psi_2$ represent the orientation angles of the parallelepiped in the zenith and azimuthal directions. Then the angular integrations are to be carried out with respect to these two angles in the form

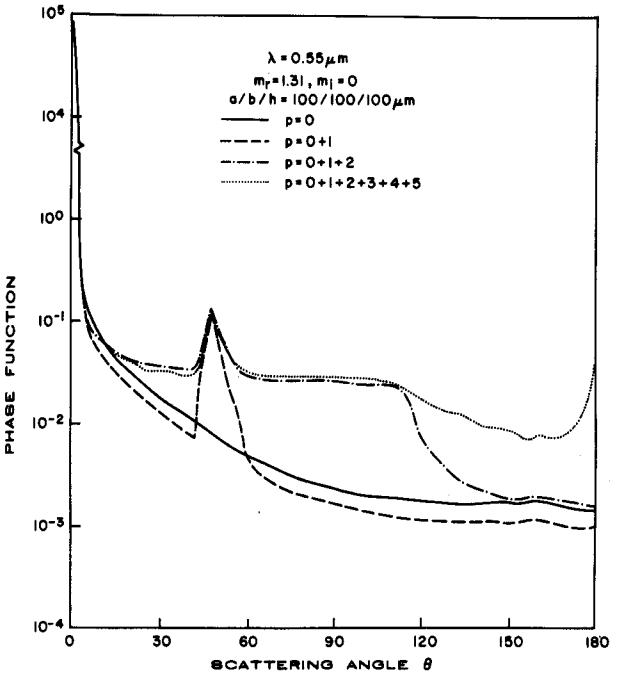


Fig. 2. Scattering phase functions for random oriented cubes with sizes of 100 $\mu$m using a wavelength of 0.55 $\mu$m and a refractive index of 1.31 corresponding to external reflection ($p = 0$), two refractions ($p = 1$), and internal reflections ($p \geq 2$).

$$P_{11}(\theta) = \frac{1}{4\pi} \int_0^{2\pi} \int_0^{\pi} P_{11}(\theta,0;\eta,\psi_2) \sin\eta d\eta d\psi_2, \qquad (12)$$

where we note that $\phi$ and $\psi_2$ are in the same azimuthal plane.[1] Moreover, the degree of linear polarization for particles randomly oriented in space is defined by

$$LP(\theta) = -\frac{P_{12}(\theta)}{P_{11}(\theta)}, \qquad (13)$$

where $P_{12}$ is angularly averaged in the same way as $P_{11}$. In the section which follows, we will present graphs for the scattering phase function and the degree of linear polarization for 3-D randomly oriented parallelepipeds and cubes.

## III. Results and Discussions

For the purpose of studying the percentage of energy associated with reflections and refractions of outgoing rays, we examine the phase functions corresponding to external reflection ($p = 0$), two refractions ($p = 1$), and internal reflections ($p \geq 2$) for randomly oriented cubes with sizes of 100 $\mu$m. A wavelength of 0.55 $\mu$m and a refractive index of 1.31 are used in the calculation. The phase function curves presented in Fig. 2 include the contribution due to diffraction, which, in the limit of geometric optics, accounts for 50% of the incident energy. The solid curve shows the normalized phase function for the combination of diffraction and external reflection. The externally reflected rays contribute to the total incident energy in an amount of ~3%. The directions of these contributions range from ~30 to 180°. The dashed curve in Fig. 2 illustrates the normalized phase function for the combination of diffraction, external reflection, and two refractions. The strong peak at the scattering angle of 46° is produced by rays undergoing two refractions through two cubic surfaces with a 90° angle. Externally reflected and two refracted rays without the diffraction contribution account for ~26% of the total incident energy. The normalized phase function due to contributions of diffraction, external reflections, two refractions, and one internal reflection is depicted in the dash–dot curve. Scattered energy in the range of ~60–120° is largely due to one internal reflection, which alone accounts for ~18% of the total incident energy. Finally, we include contributions caused by rays undergoing internal reflections up to four in the calculation of the normalized phase function, which is shown in the dotted curve. As shown, the scattered energy corresponding to scattering angles of $\gtrsim$120° is primarily contributed by internal reflections more than once. Table I depicts the total scattered energy using internal reflections up to four for various refractive indices and sizes. For the cube case, the total scattered energy for an incident energy of unity decreases as the refractive index increases. For a refractive index of 1.31, the total energy scattered from larger rectangles is less than that from cubes owing to the fact that additional internal reflections are needed for rectangles to give the same scattered energy value. As is clearly indicated in the table, the energy associated with internal reflections of more than four, which were not included in our calculations, is sufficiently small so that the calculated phase function should be quite accurate. Since the objective of presenting Table I is to examine whether four internal reflections are sufficient in the computation of the scattering phase function, calculations were not carried out for cases with dashes. The neglect of these cases is also due to the enormous amount of computer time required to complete a scattering phase function.

In Fig. 3 are shown the effects of the refractive index on the scattering phase function for randomly oriented cubes using four real refractive indices $m_r$ of 1.1, 1.31, 1.57, and 2. The distinct peak at the 16° scattering angle for the 1.1 refractive index is due to rays undergoing two refractions associated with the 90° angle of the cube. This peak reduces its magnitude as the refractive index increases. For a refractive index of 1.3, it shifts to 46°, which is known as the 46° halo in atmospheric optics. This maximum scattering feature is produced by minimum deviation rays, which undergo two reflections through a 90° angle. However, it disappears at a refractive index of $\sqrt{2}$. Thus no distinct scattering feature other than forward and backscattering peaks is shown for refractive indices of 1.57 and

**Table I. Percentage of the Total Scattered Energy for Various Refractive Indices and Sizes. The Internal Reflections up to Four are used in the Calculations**

| $m_r$ \ $a/b/h$(μm) | 100/100/100 | 100/100/1000 | 100/500/500 |
|---|---|---|---|
| 1.1 | 1.000 | — | — |
| 1.31 | 0.998 | 0.986 | 0.992 |
| 1.57 | 0.995 | — | — |
| 2 | 0.995 | 0.985 | — |

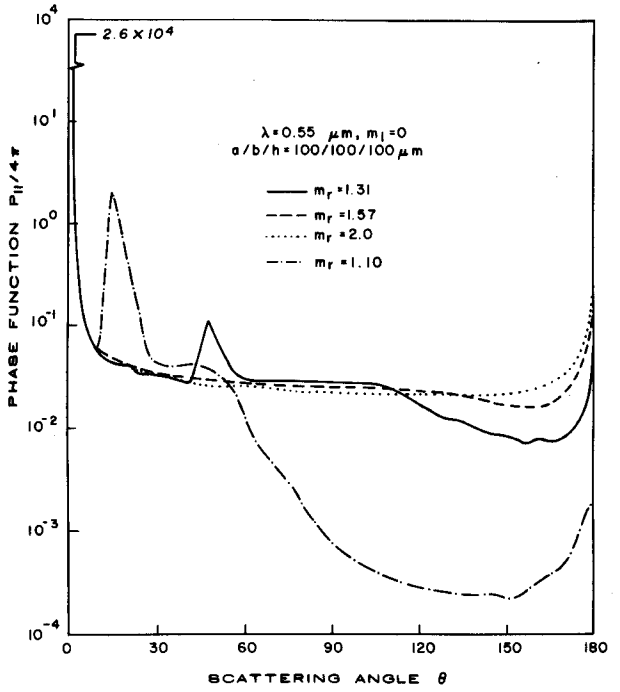


Fig. 3. Effects of the real refractive index on the scattering phase function for randomly oriented cubes as a function of the scattering angle.

2. As pointed out previously, the scattered energy in the 60–120 and 120–180° scattering angle regions are basically contributed by one internal reflection and internal reflections of more than one, respectively.

From the Fresnel reflection coefficient, it can be shown that $dE_{\text{ref}}/dm_r \approx 2m_r - 1 > 0$ for internally reflected rays, where $E_{\text{ref}}$ denotes energy associated with internal reflections; i.e., as $m_r$ increases less internal light escapes through two refraction events, and consequently more escapes through events that include reflections. Naturally, for very large values of $m_r$, almost all the light is externally reflected, and so little external light would be available. As a result, internally reflected energy increases as the refractive index increases for the range of $m_r$ values considered here. For this reason, we see that the scattering phase function for a refractive index of 1.1 in the 60–180° scattering angle region is very small when compared with other refractive indices. Moreover, the backscattering peak is seen to increase with increasing value of the refractive index.

Figure 4 illustrates the effects of the particle shape on the scattering phase function. Refractive indices of 1.31 [Fig. 4(a)] and 2 [Fig. 4(b)] are used in the calculation. In Fig. 4(a), it is seen that the diffraction peak for the aspect ratio of 1/5/5 is the largest among the three cases, since it has the largest surface area. Here we note that the effective cross-section area of scattering for randomly oriented nonspherical convex particles is one-fourth of the surface area.[7] Both 1/5/5 and 1/1/10 cases show small phase function values for scattering angles >60°. This is due to the probability of rays undergoing two refractions and internal reflections being greatest in the case of cubes. In particular, a light ray that enters one face is more likely to strike a perpendicular face in the case of a cube and hence more likely to undergo total internal reflection. However, the effect of shape on the scattering phase function for a large refractive index of 2 is less noticeable as shown in Fig. 4(b) for aspect ratios of 1/1/1 and 1/1/10. Scattering patterns for this refractive index are basically characterized by forward diffraction and backscattering with no apparent features between. Because of the higher value of $m_r$, less light escapes through two re-

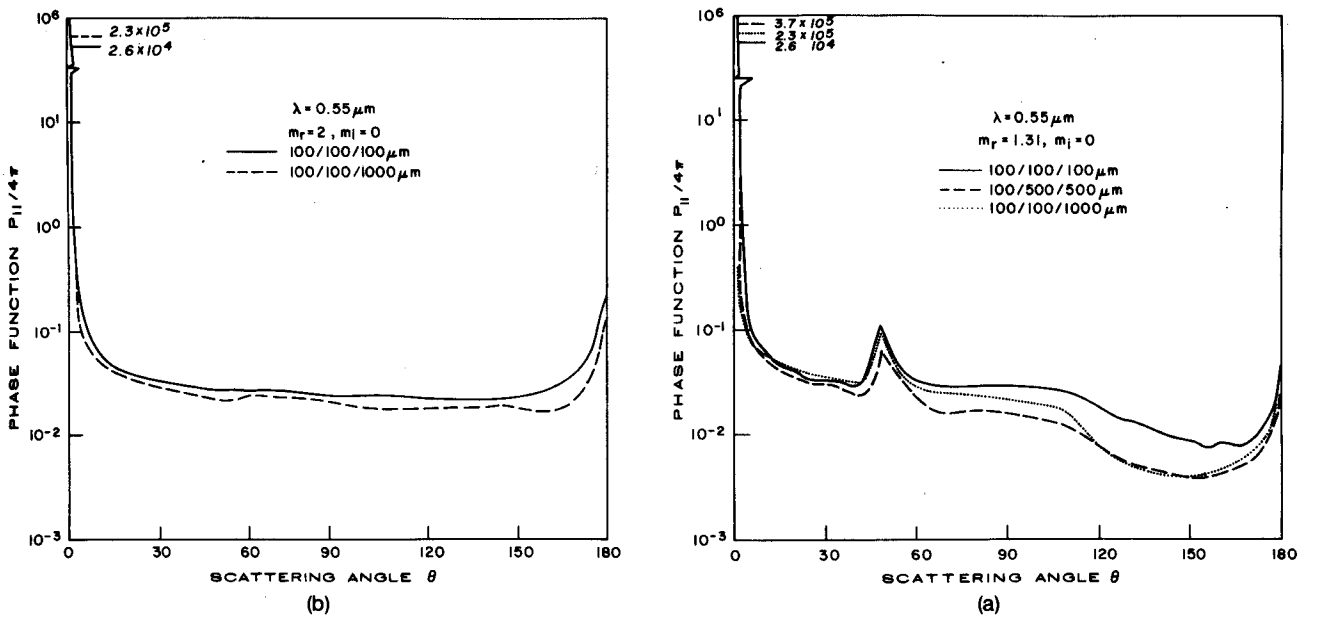


Fig. 4. Effects of the aspect ratio on the scattering phase function for randomly oriented particles as a function of the scattering angle for refractive indices of 1.31 (a) and 2 (b).

fractions, and so refraction events dominate the phase function, even for elongated geometrics.

The effect of absorption for randomly oriented cubes on the scattering phase function is examined in Fig. 5(a). The size of the cube in this study is 2 $\mu$m with an incident wavelength of 0.55 $\mu$m, a real refractive index of 1.57, and two imaginary parts of 0.006 and 0.1. In the 0.1 case, large internal absorption takes place so that most of the refracted and internally reflected rays are absorbed within the cube. This explains the lower values of the scattering phase function in the scattering angle region from 30 to 180°. For the 0.006 case, internal absorption is rather small so that the shape of the scattering phase function in the 30–60° region is very close to the curve depicted in Fig. 3 where a size of 100 $\mu$m is used for the cube. The diffraction pattern is independent of the refractive index, and, if the contribution of the geometric reflection and refraction were not considered, it should have been the same for the two absorption cases. However, the size parameter considered is rather small ($4a/\lambda \sim 15$). Because of the use of geometric ray tracing in the scattering phase function calculation, external reflection and two refractions contribute equally significantly to the scattered energy in forward directions as compared with diffraction contributions. As shown in this figure, the scattering phase function at the 0° scattering angle for the 0.006 case has a larger value than that for the 0.1 case. The reason for this is that rays undergoing two refractions normal to the cube have larger contributions to the scattered energy in the small absorption case.

In a recent study on the scattering by nonspherical particles with sizes comparable to the incident wavelength, Pollack and Cuzzi[3] developed a semiempirical theory for the calculation of the scattering phase function based on simple physical principles and parametrization of available laboratory experimental data. In particular, their phase function for particles having a circumference to a wavelength ratio of greater than several consisted of the sum of a diffraction component, an external reflection component calculated with geometric optics, and a parametrized internal transmission component. In their report, comparisons were carried out for the scattering phase function derived from their theory and from analog measurements for randomly oriented cubes of various sizes reported by Zerull and Giese.[8] In Fig. 5(b), we produce their comparison results with two additional phase functions calculated from the present geometric ray tracing program. The present study includes computations for 1/1/1- and 2/2/2-$\mu$m sized cubes randomly oriented in space with an incident wavelength of 0.55 $\mu$m. The size parameter for the former is ~7.5, while the latter is twice this value. Comparison of the present results with observed analog data in the scattering angle region from 60 to 180° shows a fairly good agreement, especially in the backscattering parts (90–120°; 150–180°), where Pollack and Cuzzi's semiempirical theory produces slightly smaller values. Scattering measurements involving NaCl cubes ($m_r$ = 1.54, $m_i$ = 0) presented by Perry *et al.*[9] and Kirmaci and Ward[10] also show a gradual increase of the scattering phase function for scattering angles >120°, which is

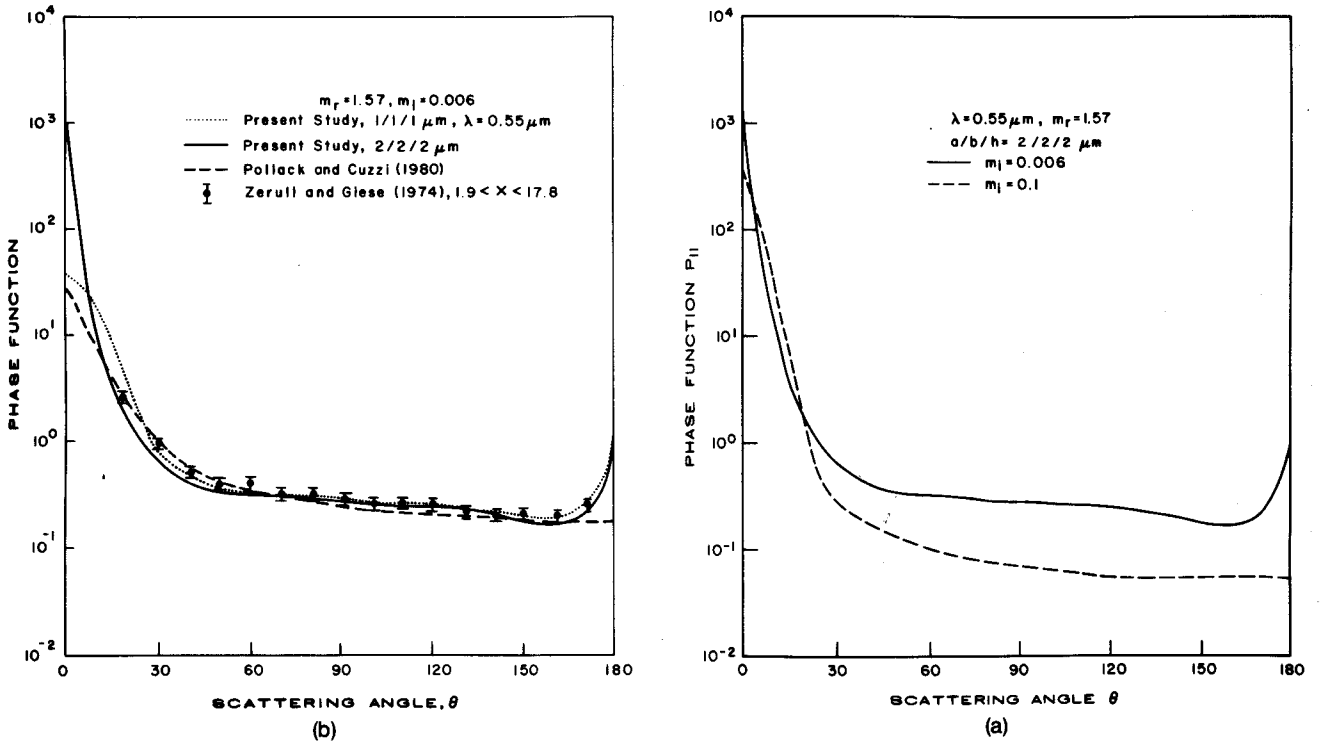


Fig. 5. (a) Effects of the imaginary refractive index on the scattering phase function for randomly oriented cubes as a function of the scattering angle using a real refractive index of 1.57. (b) Comparisons of the present results with those calculated by Pollack and Cuzzi based on a semiempirical theory and measured by Zerull and Giese from a microwave analog experiment.

Table II. Single-Scattering Albedos $\tilde{\omega}_0$ and Asymmetry Factors $g$ for Randomly Oriented Cubes with a Real Refractive Index of 1.57

| $a/b/h$ ($\mu$m) / $m_i$ | 1/1/1 | 2/2/2 | 100/100/100 |
|---|---|---|---|
| 0 | — | — | $\tilde{\omega}_0 = 1$<br>$g = 0.995$ |
| 0.006 | $\tilde{\omega}_0 = 0.926$<br>$g = 0.632$ | $\tilde{\omega}_0 = 0.870$<br>$g = 0.737$ | — |
| 0.1 | — | $\tilde{\omega}_0 = 0.555$<br>$g = 0.920$ | — |

consistent with results of Zerull and Giese. The present results, however, approximately bracket the analog data in the forward diffraction region. A slightly better fit could have been obtained by computing the diffraction component for the actual size distribution function based on the experiment. The good agreement between our computed phase function and the experimental data, especially at intermediate and backscattering angles, encourages us to think that our calculations are useful at much smaller values of the size parameter than ones for which geometric optics are strictly valid.

In Table II, we list the single-scattering albedo and asymmetry factor for randomly oriented cubes having a real refractive index of 1.57 utilizing the scattering phase function presented previously. These two basic scattering parameters, which are most important in radiative transfer analyses, are defined, respectively, by

$$\tilde{\omega}_0 = \sigma_{sca}/\sigma_{ext},$$

$$g = \frac{1}{2}\int_{-1}^{1} P(\cos\theta)\cos\theta d\cos\theta,$$

where $\sigma_{sca}$ and $\sigma_{ext}$ are the scattering and extinction cross sections, both of which along with the scattering phase function are derived from the geometric ray tracing program. For the no absorption case, the asymmetry factor has a large value of 0.995 for 100-$\mu$m cubes because of the domination of forward scattering. For large absorption ($m_i = 0.1$), the single-scattering albedo has a value of 0.555, and the asymmetry factor is also quite large because of the contribution of forward scattering. For $m_i = 0.006$, the two cubes in the calculation show a physically consistent pattern, i.e., the decrease of the single-scattering albedo and the increase of the $g$ factor as the particle size increases. In comparison with the results of Pollack and Cuzzi,[3] a smaller $g$ (0.560) than the present value for 1-$\mu$m sized cubes (0.632) is found because of the smaller diffraction peak [see Fig. 5(b)] derived in their analysis. They also presented the $g$ factor for equivalent spheres, which has a value of 0.690. Clearly, the asymmetry factor for randomly oriented cubes, which represents the relative strength of forward scattering, would be overestimated if equivalent spheres were substituted in the calculation. Because of the enormous amount of computer time required for the single-scattering calculation involving cubes by means of the ray tracing technique, cases denoted by dashes were not computed. In any event, it suffices to understand from the values presented in this table the behavior of the single-scattering albedo and asymmetry factor as functions of $m_i$ and the size of the cube. While we do compare single-scattering results for small cubes with those for equivalent spheres as presented by Pollack and Cuzzi,[3] we have not performed comparisons for large cubes. In the context of geometric optics, the scattering phase function for spheres is generally characterized by the sharp diffraction peak, rainbow features, and backscattering peak (see, e.g., results presented by Liou and Hansen[11] for $m_r = 1.33$ and 1.50). Thus comparisons of the scattering phase functions involving large cubes and parallelepipeds and equivalent spheres will not provide additional physical insight. However, we will depict the linear polarization curve for spheres and compare it with results for cubes, parallelepipeds, and columns.

Figure 6(a) shows comparisons of the degree of linear polarization for randomly oriented cubes using four different refractive indices. For the 1.1 case, a larger polarization peak with a value of ~80% is shown at the scattering angle of ~105°. This peak is clearly associated with rays undergoing external reflections, since in the 60–150° scattering angle region the scattered energy due to internal reflections is insignificant, as pointed out previously. Negative polarization is shown for the 16° halolike peak and in backscattering directions. As the refractive index increass to 1.31, which is the refractive index for ice, the linear polarization pattern shows considerable structure over the full range of scattering angles. Negative polarization is seen at the 46° halo, as it is in the case of hexagons. Small positive polarization (~10%) is seen in the forward directions and in the 120–140° scattering angle region. Strong negative polarization is produced in backscattering directions with a maximum value of 50% at a scattering angle of ~176°. The polarization patterns are randomly oriented cubes having a refractive index greater than $\sqrt{2}$ exhibit similar but broader features, i.e., broad maximum in the 30–40° scattering angle region and a negative peak at an ~175° scattering angle. The positive maximum and negative minimum as well as the zero polarization cross point shift to larger scattering angles as the refractive index increases. Increasing the refractive index increases the positive polarization maximum in forward directions, and the reverse is true in backscattering directions. Much of these polarization patterns reflect the competition between positively polarized externally reflected light and negatively polarized externally transmitted light.

Figure 6(b) illustrates the effect of internal absorption on the scattered polarization pattern for randomly oriented cubes using a real refractive index of 1.57. The incident wavelength is 0.55 $\mu$m, and the size of the cube is 2 $\mu$m. For the large absorption case ($m_i = 0.1$), the linear polarization pattern is basically produced by external reflections except in the region from 0 to 30° scattering angle where two refractions also make a significant contribution to the scattered energy as is evident from Fig. 5(a). The maximum positive polarization occurs at a scattering angle of ~70° for $m_r = 1.57$. For the small absorption case ($m_i = 0.006$), two refractions and one internal reflection make significant con-

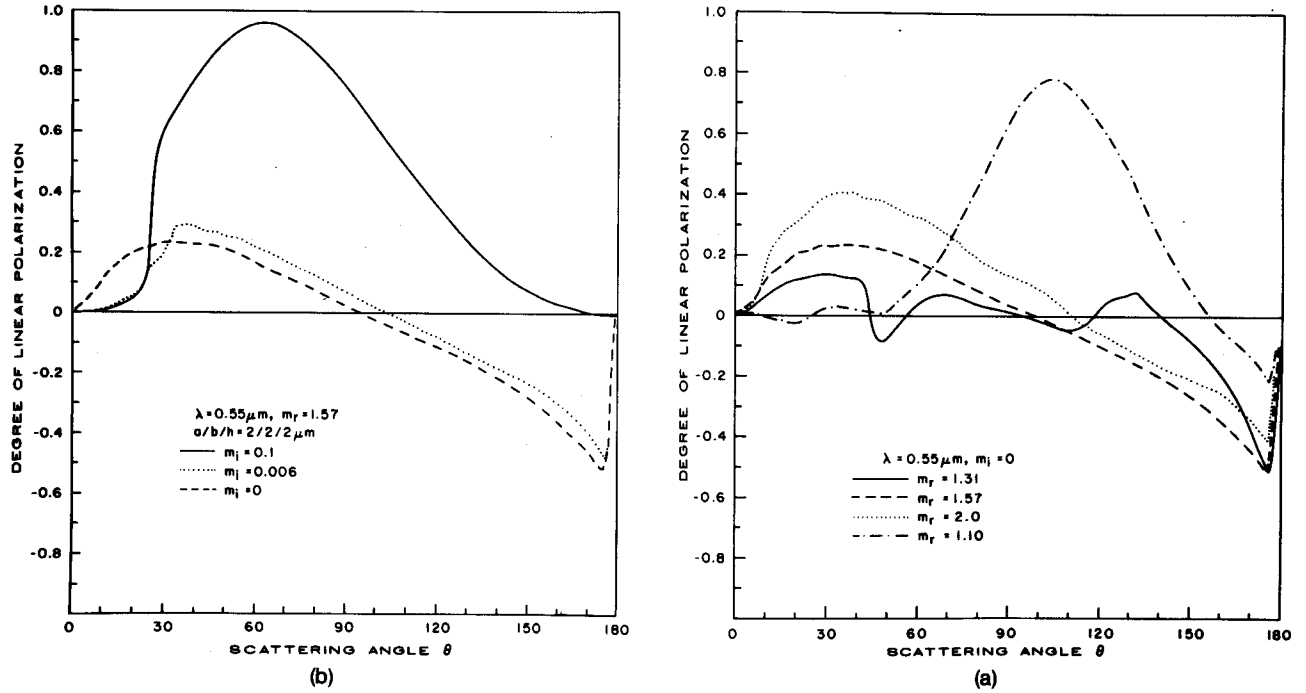


Fig. 6. Effects of the real $m_r$ and imaginary $m_i$ refractive index on the degree of linear polarization for randomly oriented cubes as a function of the scattering angle: (a) real part ($m_i = 0$); (b) imaginary part ($m_r = 1.57$).

tributions in the 30–180° scattering angle region. As a result, positive polarization is greatly reduced. Except in the 0–30° region, its polarization pattern resembles that of no absorption. Generally, as the imaginary refractive index increases, the positive polarization increases due to the increasing dominance of externally reflected light.

Finally, we examine the influence of the particle shape on the polarization pattern. Included in Fig. 7 are polarization results for hexagonal columns with an aspect ratio of $a/L = 1/5$, where $a$ and $L$ are the radius and length, respectively, presented by CL and for spheres presented by Liou and Hansen,[11] both of which are derived by means of a geometric ray tracing program. The linear polarization pattern of randomly oriented rectangular parallelepipeds closely resembles that of cubes with larger positive values from 0 to 140° scattering angles. Rectangular parallelepipeds produce double-negative maxima in backscattering directions, while cubes show a single-negative peak located at the 176° scattering angle. When both results are compared with hexagonal cylinders, a number of significant differences are seen. These include negative polarization at the 22° halo and larger positive polarization in the 90–120° scattering angle range produced in the hexagon case. Both rectangular and hexagonally shaped particles generate a maximum at an ~130° scattering angle, which is associated with rays undergoing two internal reflections. In CL, comparisons between the computed and measured degree of linear polarization have been made for plates and columns. It is shown that the computed linear polarization for 20-μm plates closely matches the experimental data for plates having a

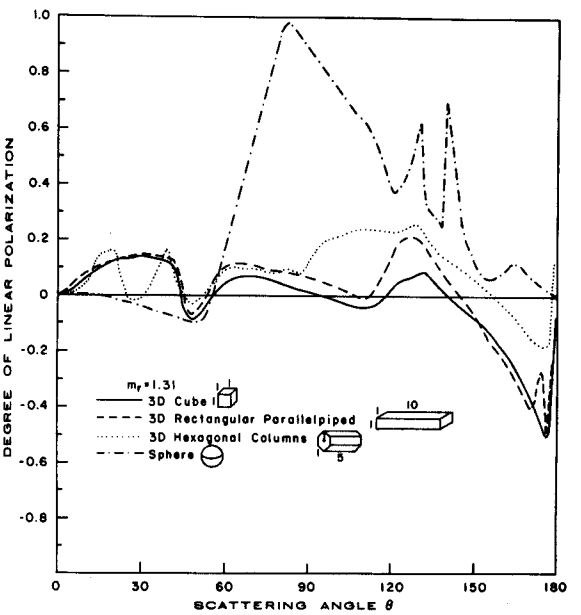


Fig. 7. Influence of the particle shape on the linear polarization pattern as a function of the scattering angle. Included for comparisons in the figure are cubes, parallelepipeds, hexagons, and spheres. All the polarization curves are computed from geometric ray tracing programs.

modal diameter of ~5 μm.[12] Scattering and polarization patterns for cubes, rectangular parallelepipeds, and hexagonal cylinders deviate greatly from those for spheres as is well illustrated in this figure. In the limit of geometric optics, spheres produce a maximum at a scattering angle of ~80°, which is generated by external

reflections. The peaks at about the 140 (primary rainbow) and 130° (secondary rainbow) scattering angles are caused by rays which undergo one and two internal reflections, respectively.[11] As the size of the sphere decreases, it is noted that the maximum produced by external reflection gradually disappears. Other interesting polarization differences between spherical and nonspherical particles are noted in the 0–40 and 150–180° scattering angle regions where the sign of polarization is reversed.

## IV. Summary

In this paper we have extended the geometric ray tracing theory for the scattering of hexagonal cylinders derived by CL to cubes and rectangular parallelepipeds. Calculations have been carried out to investigate the effects of real and imaginary parts of the refractive index on the scattering phase function and the degree of linear polarization for randomly oriented cubes. The effects of the aspect ratio of randomly oriented parallelepipeds on the scattering and polarization patterns are also examined. Below is a summary of significant findings from the present study:

(1) Using the real refractive indices $m_r$ of 1.1, 1.31, 1.57, and randomly oriented cubes, we find that the scattered energy in the 60–180° scattering angle, which is produced largely by internal reflections, reduces as $m_r$ decreases (Fig. 3). The low scattering angle halo feature produced by light rays undergoing two refractions through an angle of 90° disappears for $m_r \geq \sqrt{2}$.

(2) Rectangular parallelepipeds scatter less energy than cubes in scattering angles of >60° for a refractive index of 1.31. However, differences become insignificant for a larger refractive index of 2 (Fig. 4).

(3) Comparisons of the phase function from the present program for cubes with that derived by Pollack and Cuzzi[3] based on a semiempirical theory reveal that the phase function in the scattering angle regions of 90–120 and 150–180° is slightly improved by performing the geometric optics calculations much more rigorously when both are compared with the measured data presented by Zerull and Giese[8] (Fig. 5). As noted earlier, the good agreement between our calculations and the laboratory data may imply that phase functions calculated by diffraction/geometric optics theory may provide a good approximation to the phase function of randomly oriented nonspherical particles, even for size parameters as small as ~10.

(4) For real refractive indices of $>\sqrt{2}$, linear polarization patterns for randomly oriented cubes exhibit similar features including a broad maximum in the 30–40° scattering angle region and a negative peak around a scattering angle of 175° (Fig. 6). For a real and imaginary refractive index of 1.57 and 0.1, it is shown that the linear polarization pattern is dominated by external reflections with a maximum positive polarization at about ~70 scattering angle.

(5) Using a real refractive index of 1.31, we show that the polarization patterns for cubes and parallelepipeds are extremely similar. However, they both differ significantly from that for hexagonal cylinders in the 22° halo and 90–120° scattering angle regions (Fig. 7). These nonspherical particles do not generate maximum positive polarization in the rainbow regions, which are typical for the scattering of light by spheres. Spheres, on the other hand, will not produce halo features which exhibit negative polarization.

The above findings appear to be of significance for the interpretation of observed scattering and polarization data to identify the shape and optical property of cloud and aerosol particles in planetary atmospheres. Moreover, the present single-scattering phase function and polarization information should also be useful for understanding the transfer of radiation in an atmosphere containing nonspherical particles.

## References


1. S. Asano and M. Sato, Appl. Opt. **19,** 962 (1980).
2. P. W. Barber and C. Yeh, Appl. Opt. **14,** 2864 (1975).
3. J. B. Pollack and J. N. Cuzzi, J. Atmos. Sci. **37,** 868 (1980).
4. Q. Cai and K.-N. Liou, Appl. Opt. **21,** 3569 (1982).
5. K. N. Liou, *An Introduction to Atmospheric Radiation* (Academic, New York, 1980), p. 146.
6. H. C. van de Hulst, *Light Scattering by Small Particles* (Wiley, New York, 1957), p. 43.
7. V. Vonk, Nature London **162,** 330 (1948).
8. R. H. Zerull and R. H. Giese, in *Planets, Stars and Nebulae Studied with Photopolarimetry*, T. Gehrels, Ed. (U. Arizona Press, Tucson, 1974), p. 901.
9. R. J. Perry, A. J. Hunt, and D. R. Huffman, Appl. Opt. **17,** 2700 (1978).
10. I. Kirmaci and G. Ward, Appl. Opt. **18,** 3328 (1979).
11. K. N. Liou and J. E. Hansen, J. Atmos. Sci. **28,** 995 (1971).
12. K. Sassen and K. N. Liou, J. Atmos. Sci. **36,** 852 (1979).



This research was supported in part by the NASA Ames Consortium contract SST-1279/T-3892 and the Division of the Atmospheric Sciences, National Science Foundation grant ATM81-09050. We thank Sharon Bennett for typing and editing the manuscript. Q. Cai is on leave from the Lanzhou Institute of Plateau Atmospheric Physics, Academia Sinica, China.